CIRP Journal of Manufacturing Science and Technology 12 (2016) 79–89

Contents lists available at ScienceDirect

CIRP Journal of Manufacturing Science and Technology

journal homepage: www.elsevier.com/locate/cirpj

Experimental and numerical investigations in electro-chemical milling

S. Hinduja [a,*], J. Pattavanitch [b]

[a] School of Mechanical, Aerospace and Civil Engineering, The University of Manchester, Manchester, UK
[b] Department of Mechanical Engineering, Burapha University, Chon Buri, Thailand

ARTICLE INFO

Article history:
Available online 25 October 2015

Keywords:
ECM
Pocket milling
Modelling
BEM

ABSTRACT

This paper presents experimental and numerical investigations into electro-chemical (EC) milling of simple features such as slots and pockets. Preliminary experimental investigations into the machining of a slot enabled appropriate process parameters to be selected; these were then used to machine a simple square pocket and finally a pocket with a human-being shaped protrusion. These features were machined with tools having circular and square cross-sections. The pocket with the protrusion was machined with tool paths of zig–zag and contour-parallel type. The experimental results indicated that the machining accuracy depends upon, amongst other things, on the tool shape and process parameters. A boundary element of the EC machining process was used to predict the shape of the pockets and in most cases, the predicted shapes compared favourably with the actual machined features.

Introduction

Demand for parts made from high strength, heat and corrosion-resistant materials such as titanium and Inconel, is increasing because of their use in fields such as automotive, medical and aerospace parts. Conventional processes are not really suitable to machine these difficult-to-cut materials because the cutting tools have to be made of a material that is harder and stronger than that of the workpiece.

The disadvantage of having to use harder and stronger cutting tools can be overcome by resorting to non-conventional processes such as electrical discharge machining (EDM), laser beam machining and electrochemical machining (ECM). In EDM and laser beam machining, the stock is removed by using high thermal energy to melt the material. Although in these processes the material is removed without the tool coming into contact with the workpiece, heat-affected zone, residual stresses, and sometimes even surface cracks, are present in the workpiece.

On the other hand, ECM has the advantage that there is no heat-affected zone or residual stresses in the machined workpiece. Material is removed by electrolysis wherein the anode (workpiece) undergoes dissolution at a rate that is largely dependent on the current density. ECM has the advantage of machining materials irrespective of their hardness and toughness; the only requirement is that the material must be conducting. There is a temperature increase within the electrolyte gap due to Joule heating; however, the majority of this heat is conducted away by the bulk of the electrolyte, resulting in a very small amount of heat being conducted into the anode (workpiece).

The common applications of electro-chemical machining are drilling and die sinking. In the latter, a complex 3D shape of the cathode (tool) is reproduced in the workpiece by an axial movement of the tool. In electro-chemical drilling, the shape of the tool is axisymmetric whereas in die sinking, the shape of the tool is similar, but not identical, to that of the workpiece. A considerable effort is required to design the tool for die sinking and it is usually done by trial and error. The time and effort required to design and fabricate the tool for design is reflected in the cost of the workpiece. The difficulties of tool design in EC sinking can be mitigated to a large extent if the die could be electro-chemically machined using a tool of very simple geometry (*i.e.* having a rectangular, spherical or cylindrical cross-section), as in conventional milling, over the workpiece surface.

There has been very limited research in electro-chemical milling, both at the micro and macro scale. At the micro level, most researchers use pulsed machining and Kozak, Rajurkar and Makkar [1] were one of the first to demonstrate pulsed EC micro milling. They milled a simple slot in several axial passes using a cylindrical tool of diameter 280 μm. They also attempted to model the process analytically but were able to do so for only one pass. Use of a cylindrical tool resulted in the sidewalls of the machined feature to become tapered. Kim et al. [2] were able to overcome this disadvantage by using a disc-type electrode; they electro-chemically milled a micro open pocket the sidewalls of which

* Corresponding author. Tel.: +44 7540158207.
E-mail address: sri.hinduja@manchester.ac.uk (S. Hinduja).

http://dx.doi.org/10.1016/j.cirpj.2015.07.003
1755-5817/

were almost square to the base face. Micro features have also been milled using the recently developed electro-chemical jet process. Hackert-Oschätzchena et al. [3] electro-chemically milled slots 200 μm wide and 60 μm deep with a jet diameter of 100 μm. More recently, Zeng et al. [4] used electro-chemical milling to improve the surface of a feature previously machined by EDM. They deployed electro-chemical milling to remove the 5 μm thick re-cast layer.

At the macro scale, Kozak et al. [5] investigated the milling of flat and cylindrical surfaces, both convex and concave, with a ball-ended electrode, which they referred to as a universal tool. The main purpose of their experiments was to verify the results predicted by their analytical model. Instead of using a ball-ended cutter, Ruszaj and Zybura-Skrabalak [6] used a tool with a rectangular cross-section to mill slots and they compared the experimentally measured surface roughness values with those predicted by a computer model. Pattavanitch and Hinduja [7] also used a rectangular-shaped tool to mill deep and wide slots and they investigated the waviness of the base surface of the slots produced with different step-over distances. A numerical model using the boundary element (BE) method was also developed in order to predict the 3-D shape of slots. More recently, Vanderauwera et al. [8] also investigated the surface finish that can be obtained with electro-chemical milling. They found that the accuracy of the machined feature is improved with pulse milling.

Since several researchers have investigated electro-chemical milling of simple slots, this paper investigates the machining of more complex features at macro scale; the effect of different tool geometries and different type of tool paths are also studied.

Modelling of the ECM process has followed a similar path as the experimental research work. The initial models were confined to electro-chemical drilling and die sinking and these models used various techniques such as: the analytical methods deployed by Hewson-Browne [9] and Loutrel and Cook [10]; the finite difference method by Tipton [11] and Kozak [12]; the finite element method by Jain and Pandey [13] and Alkire, Bergh and Sani [14]; and the boundary element method by Narayanan, Hinduja and Noble [15] and Deconinck [16]. Again, BE models have been developed for electro-chemical milling [7] but only for simple slots. This paper discusses the difficulties encountered when the BE method as described in [7] is used to mill complex features.

Experimental setup

The experimental set-up consisted of a 3-axis Denford CNC milling machine, which was converted into an ECM machine. The workpiece was a rectangular bar made of SS-316 and was placed over a block of polymer that was wider than the workpiece bar (see Fig. 1(b)); both were submerged in a plastic work bath of electrolyte as shown in Fig. 1(a). The electrolyte was sodium nitrate ($NaNO_3$) (10% by weight in water). The tool was held in the spindle of the Denford CNC machine, the spindle being held stationary. A DC voltage was applied between the tool and the workpiece. A data acquisition system was used to record the voltage and current.

Two tools of different shapes were used in the investigations (see Fig. 2). These tools were made from copper; one had a square cross-section of size 1 × 1 mm and the other tool a circular cross-section of radius 0.5 mm.

BE model for electro-chemical milling

Although there were three components *i.e.* tool, workpiece and insulating block (see Fig. 1(b)), the BE method required only the outer surfaces of the tool and the workpiece to be modelled. For the tool, an open shell was formed by the end and side faces (oranges

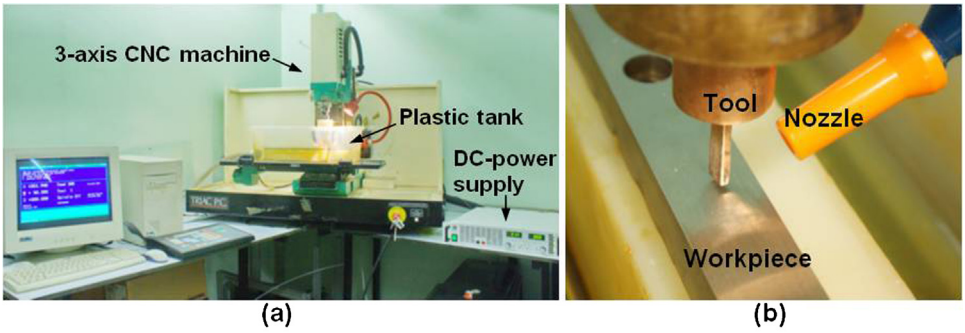

Fig. 1. (a) Three-axis ECM milling machine and DC power supply and (b) The tool, workpiece and nozzle.

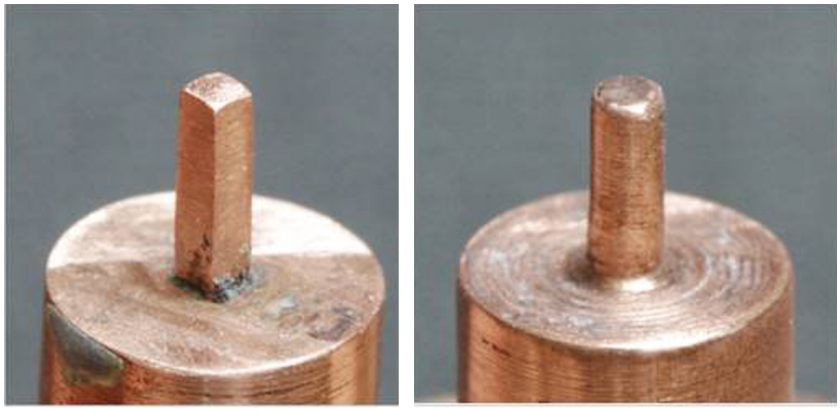

Fig. 2. Square and cylindrical tools.

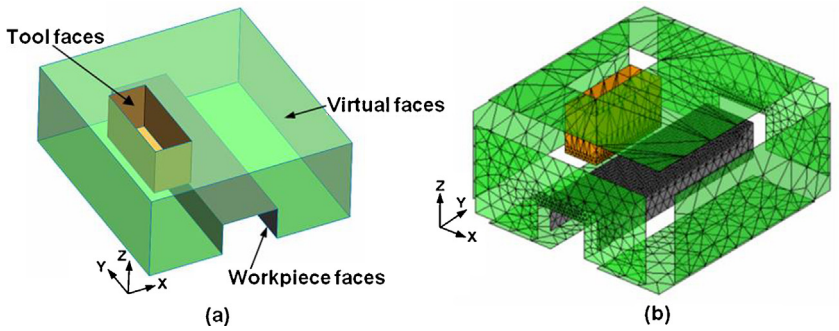

Fig. 3. (a) BE domain for EC milling and (b) the complete discretised 3D domain.

faces in Fig. 3(a)) and for the workpiece, an open shell was formed by the top and side faces (grey faces in Fig. 3(a)). These open shells were then connected by virtual faces (green faces in Fig. 3(a)) to form a closed shell. These virtual faces were sufficiently far away from the top face of the workpiece and the end face of the tool and therefore did not affect the computed values of the current density distribution between the tool end face (cathode) and workpiece top face (anode).

The analysis domain was discretised using linear triangular elements. A graded mesh was used for the side surfaces of the tool and workpiece, the mesh being fine near the top face of the workpiece and the end face of the tool. Since the virtual surfaces have no effect on the predicted shape of the workpiece, they were discretised with coarse unstructured meshes. The complete mesh is shown in Fig. 3(b).

The current flux was calculated at each node by solving Laplace's equation within the domain formed by the closed shell.

$$\nabla^2 U = 0 \tag{1}$$

It was assumed that the electrolyte's electrical conductivity did not change due to Joule heating of the electrolyte. This is a valid assumption since, unlike EC drilling, a sufficiently large quantity of electrolyte was pumped through the nozzle and into the inter-electrode gap; furthermore, the amount of electrolyte contained in the work tank was significantly large thus ensuring that the electrolyte leaving the inter-electrode gap achieved ambient temperature quickly.

The over-potential was assumed to be independent of the current density and this assumption is reasonable since the inter-electrode gap for the experiments was 0.2 mm. The total over-potential was determined experimentally as 1.5 V and hence the voltage (U) on the top and side faces of the workpiece was assumed to be ($V-1.5$) volts where V is the applied voltage. The side faces of the tool were bare, hence the end and side tool faces of the tool were assumed to be at 0 V. The virtual surfaces were sufficiently far away from the tool and top surface of the workpiece and therefore they were insulated (*i.e.* $dV/dn = 0$).

In continuous electro-chemical milling, the tool is moved continuously in the feed direction. To simulate this temporal problem, the tool was moved by a distance traversed in Δt seconds and with the tool in this position, an analysis was performed assuming steady state conditions. The analysis provided updated values of the current density $J(J = \kappa_e dU/dn)$ at each node. Based on Faraday's law the workpiece shape after each time step was determined by moving each node by a distance Δh in a direction normal to the surface of the node [17].

$$\Delta h = \varepsilon \frac{M \times J \times \Delta t}{\rho \times z \times F} \tag{2}$$

where M is the atomic weight of workpiece material, F the Faraday's constant, z the valency, ε the current efficiency, κ_e the electrolyte's electrical conductivity and ρ the workpiece material density.

The changing shape of the workpiece caused some of the triangular elements on the workpiece surface to get stretched and others compressed, resulting in the mesh becoming distorted. Therefore, even though the quality of the initial mesh on the workpiece surface was good, it quickly deteriorated and its quality and density had to be improved after every few time steps. Also at the end of every time step, the tool surfaces had to be translated and the mesh on the top virtual surface regenerated. Furthermore, since the slot and pocket were machined in more than one axial pass, then at the end of each pass, the tool surfaces and the top virtual surface were translated towards the workpiece surface by the axial depth.

Experimental results

Machining a deep slot

Preliminary investigations

Initial investigations were conducted to determine the process parameters, which would result in the smallest overcut. In these tests, a slot was machined in a single pass using the 1×1 mm square cross-section copper tool. This slot was machined at three different feed rates, ranging from 3 to 9 mm/min and three different applied voltages, ranging from 6 to 14 V, with the initial inter-electrode gap being 0.2 mm. A full factorial analysis was performed and the depth and width of the machined slots are shown in Table 1.

From the results, it is clear that for a particular value of applied voltage, the depth and width of the slot increase when the tool feed rate decreases. This is to be expected because, with decreasing feed rate, a unit area of the workpiece sees the tool for a longer time. On the other hand, at a specified feed rate, both the width and depth increase with increasing applied voltage. This is reasonable since an increased applied voltage results in a corresponding increase in the current density, causing a greater amount of material dissolution. Obviously the minimum overcut corresponds to a slot with the minimum width and this was obtained with the feed rate of 9 mm/min and applied voltage of 6 V, the resulting width and depth of the slot being 1.17 and 0.021 mm, respectively.

Table 1
The depth and width of single slot machined at different conditions.

		Applied voltage (V)					
		14		10		6	
		Depth	Width	Depth	Width	Depth	Width
Feed rate (mm/min)	3	0.14	2.24	0.098	2.02	0.032	1.35
	6	0.08	1.91	0.048	1.79	0.026	1.29
	9	0.049	1.82	0.04	1.69	0.021	1.17

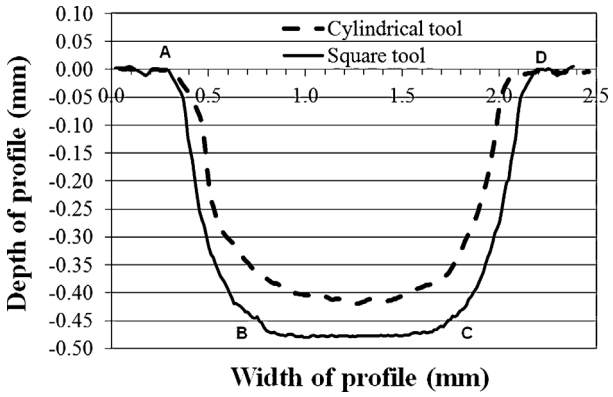

Fig. 4. Profile of the slot after 25th axial passes. (For interpretation of the references to colour in this figure legend, the reader is referred to the web version of this article.)

Effect of tool geometry

To investigate the effect of tool geometry on the shape of the machined slot, two tools, one with a circular cross-section and the other with a square, were used to machine a deep slot. The cylindrical tool had a radius of 0.5 mm and the square tool a side of 1 mm. Both these tools were not insulated and the applied voltage and feed rate were as discussed in the previous section. As before, the initial gap was 0.2 mm. The slot was machined in 25 axial passes, the axial depth in each pass being 0.02 mm. When machining, the tools were moved along the length of the slots at varying feed rates but unlike conventional milling, the tools were not rotated (see Fig. 6).

The cross-sectional profiles of the slots machined by the square and cylindrical tools after the twenty-fifth axial pass are shown in Figs. 4 and 5. The cross-sectional shapes shown in Fig. 4 were measured using a laser profiler machine.

The sidewalls (AB and CD, Fig. 4) of the slot machined by the square tool after 25 passes were tapered and the base of the slot (from B to C) was almost flat. There was no distinct edge defining the junction between the sidewalls and base face, instead there was a blend between the two. In the case of the cylindrical tool, the base face of the slot was curved; see the cross-sectional profile in Fig. 5(b). The sidewalls, however, were also tapered but the width of the slot was smaller than that obtained with the square tool.

The width and depth of the slot after the 1st, 14th and 25th pass are shown in Table 2. The results clearly show that the width and depth of the slots machined by the cylindrical tool are smaller than those machined by the square tool.

Table 2
The width and depth of slot obtained experimentally.

	Width of slot (mm)			Depth of slot (mm)		
Number of tool passes	1	14	25	1	14	25
Square tool shape	1.17	1.54	1.85	0.021	0.20	0.48
Cylindrical tool shape	1.15	1.30	1.46	0.013	0.17	0.41

Also the overcut is not the same per pass. Take for example the square tool. In the first pass the overcut is 0.085 mm. But at the end of the 14th pass, the width of the slot is 1.54 mm, which means that the slot has increased in width in the last 13 passes by 0.37 mm. Hence the average overcut per pass is $0.37/(13 \times 2) = 0.01423$ mm which is a sixth of the value for the first pass. A similar calculation of the average overcut from the 14th to the 25th pass results in a value of 0.0141 mm. This seems to suggest that the overcut has converged to a value around 0.14 mm. However, this is not the case for the frontal gap which at the end of the first pass is 0.221 mm for the square tool. It then decreases to 0.12 mm at the end of the 14th pass but then increases to 0.18 mm at the end of the 25th pass. The results for the cylindrical tool followed a similar pattern, the frontal gap after the 1st, 14th and the 25th pass being 0.213, 0.09 and 0.11 mm.

To explain these results, consider the machining of slot ABCD (see Fig. 6) and line *P*–*P* lying on the base of the slot and just ahead of the circular cutter. Consider a point lying on line *P*–*P* on the workpiece surface; if one assumes that material at and around this point undergoes dissolution only when it is within the projected area of the tool, then the depth of material machined at this point will be directly proportional to the time that the point is within the circular area of the tool. Hence, as the tool is fed through from *E* to *E*′, point 3 on this line will be within the tool's circular cross-section area for the time it takes to traverse one diameter of the tool; hence point 3 will be under the projected area of the tool longer than any other point on line *P*–*P* and therefore the maximum depth will occur at point 3. On the other hand, points 1 and 5 will be within the circular area for a very short time and the minimum depth will occur at these points. Hence it is not surprising that the base face of the slot is curved.

In the case of the square tool, all the points on line *P*–*P* will be within the cross-sectional area of the tool for the same amount of time and therefore the same amount of material will be removed at all points on this line. Hence the base face of the slot should be flat.

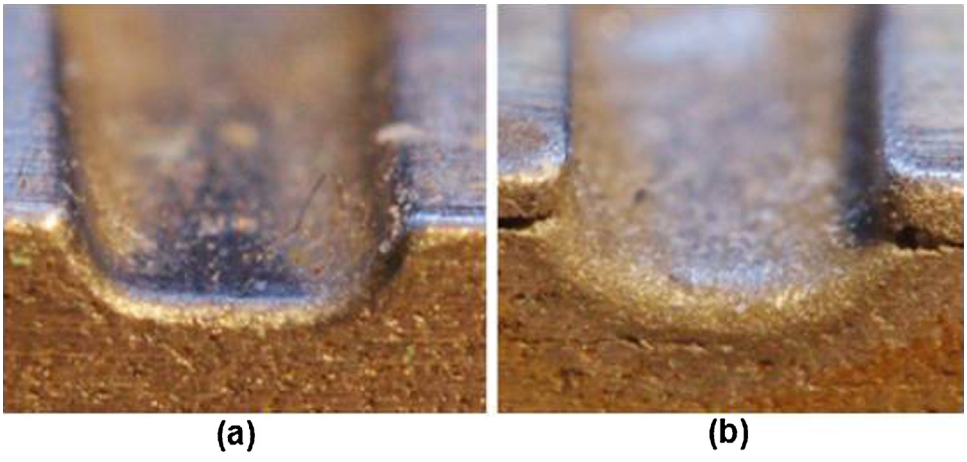

Fig. 5. A 3D view of the slot machined using (a) square and (b) cylindrical tools.

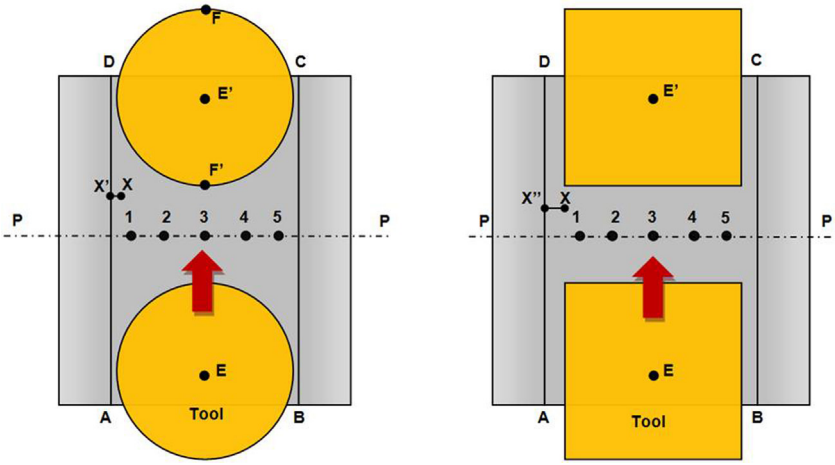

Fig. 6. Profile *P–P* when machining with a cylindrical and rectangular tool.

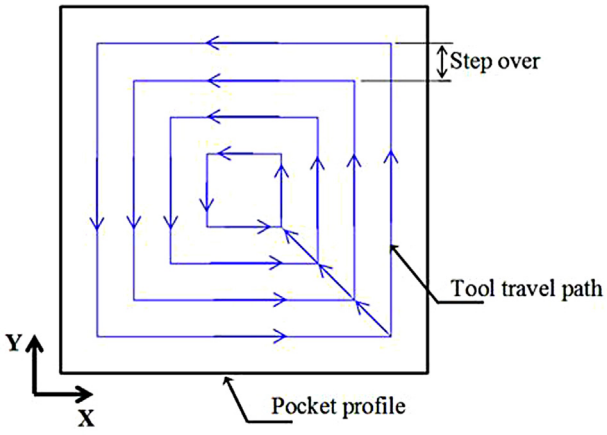

Fig. 7. Tool path for rectangular pocket.

In Fig. 4, the width of the slot machined by the square tool is wider than that machined by the cylindrical tool. In ECM, the tool also machines material that lies on the sidewalls of the slot due to stray currents. The amount of material removed depends on the tool shape. Consider a point X on the sidewall AD (Fig. 6). When this sidewall is machined by a circular tool, this point will be in line with the tool only for an instant. Immediately before and after this, it will experience some dissolution due to stray machining; let X' be the new position of point X after the tool has travelled past it. On the other hand, when the sidewall is machined by a square tool, the same point will be directly in line with the side face of the tool for a much longer time. Therefore, the amount of machining at this point will be greater *i.e.* $X–X'' > X–X'$. This will result in the width of the slot, when machined by a square tool, to be much greater than that with a cylindrical tool.

Since the tools used were bare, current did flow not only from the end face of the tool but also from its side, front and back faces. Since the slot was machined in several axial depths, material at the very top of the side surfaces would have been machined by the tool several times, whereas the material at the very bottom of the side surface would have been machined by the tool only once and this caused the side faces of slots machined with a bare tool to be tapered.

Machining a square pocket

The results of machining a square pocket with square and cylindrical tools are described in this section. The square pocket was of size 5 × 5 mm and was machined using a spiral-in type tool path with a step-over distance of 0.1 mm (see Fig. 7). The pocket was machined using 24 axial passes using the same conditions as when machining the deep slot.

Two views of the pocket machined by the cylindrical tool are shown in Fig. 8 whereas Fig. 9 shows the same pocket when machined by the square tool. The cross-section profiles of the pockets machined by the tools are shown in Fig. 10; the shapes are similar with the slot machined by the square tool deeper and wider. The bottom surfaces are flat and, as expected, the sidewalls are not vertical. The junction between the sidewalls and the base surface is rounded. The width and depth are 6.06 mm and 0.63 mm for the slot machined by the square tool and 5.86 mm and 0.6 mm with the cylindrical tool. Hence, the square tool machines a bigger pocket than the cylindrical tool. Although the square tool results in

Fig. 8. Pocket machined by a cylindrical tool.

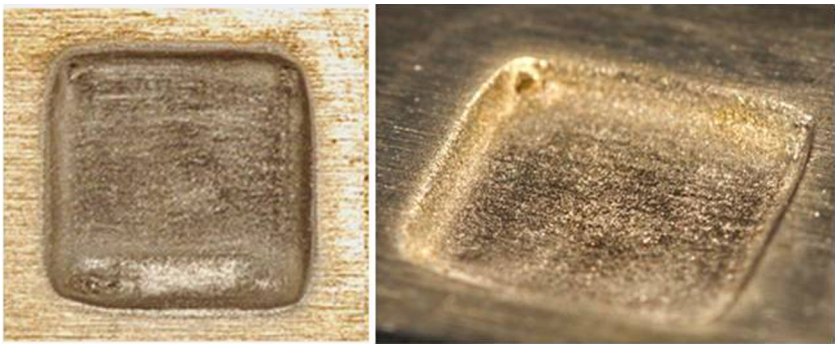

Fig. 9. Pocket machined by a square tool.

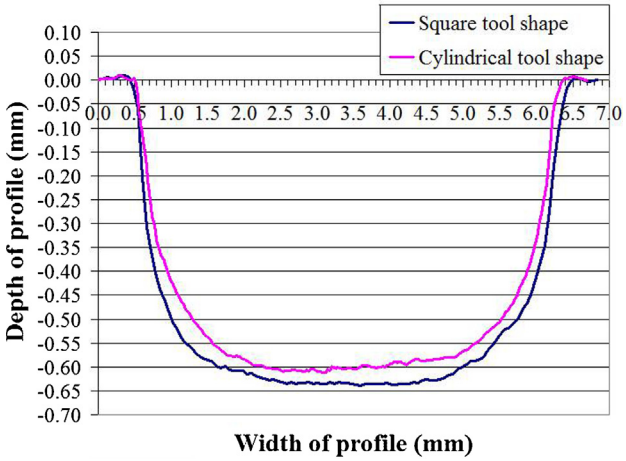

Fig. 10. The profile of pockets machined with different tool shapes.

the base face of the pocket having sharper edges, the corners of the pocket are rounded (Fig. 9). This is because there are current flux lines emanating from the tool corner to the workpiece.

Pocket with human-shaped protrusion machining

To further investigate whether EC milling is capable of machining more complex features, a pocket with a protrusion in the shape of a human being was machined. This pocket (see Fig. 11(a) has been considerably modified from the original milling pocket proposed by Held [18] and the pocket for which optimum milling tool paths were generated by Hinduja, Mansor and Owodunni [19]. The depth of the pocket was also reduced to 0.5 mm to limit the number of axial passes required. In spite of this, twenty-four axial passes were required to machine the pocket, each pass being 0.02 mm. Because the internal and external boundaries of the pocket contain circular arcs, only the cylindrical tool was used. Since the smallest concave fillet radius on the protrusion is 1 mm, it was possible to use the same cylindrical tool described earlier.

There is no commercially available software specially tailored to generate tool paths for EC milling. The options available were to either generate the paths manually or to use commercially available software normally used for machining milled components. The first option was not considered because of the complex shape of the human-figured protrusion. The second option was chosen even though it was known *a priori* that the tool paths generated would not be ideally suited for ECM.

MASTERCAM was chosen and it was able to generate different types of tool paths *i.e.* zig, zigzag, and contour-parallel. The latter can either start from the external boundary and then spiral in towards the protrusion. Alternatively the paths could start from the inner boundary and then spiral outwards. Zig tool paths were not considered because the paths would have been discontinuous involving tool lifting and rapid movements. Therefore, only the effect of zigzag and spiral-in tool paths were investigated (Fig. 12). Previous investigations have shown that a radial offset of 0.1 mm produced a good quality surface [6] and therefore this value was

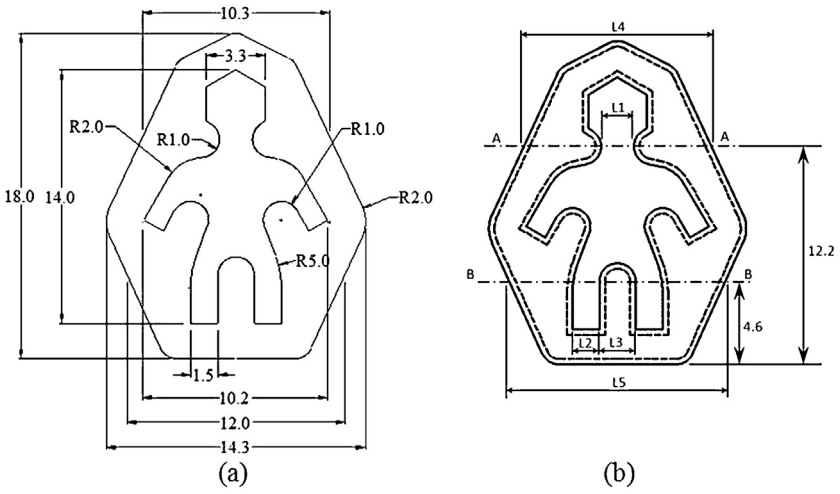

Fig. 11. (a) Pocket with a human-shaped protrusion and (b) The offset profile of human-shaped protrusion.

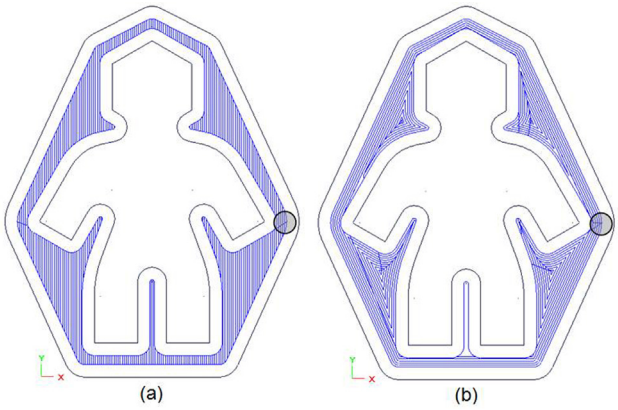

Fig. 12. (a) Zig–zag and (b) contour-parallel tool paths.

used to generate zigzag and spiral-in tool paths. For each axial pass, the lengths of the zigzag and spiral-in tool paths were 553.4 mm and 608.3 mm, respectively, and the machining times, with a feed rate of 9 mm/min, were 62 and 68 min approximately.

Electro-chemical milling is different from conventional milling in the sense that the tool is not moved along the boundaries of the feature. To machine a feature accurately, the tool must be at a distance away from the boundary by the overcut. In the case of the pocket, the profile of the protrusion was offset outwards and the outer boundary of the pocket inwards by the overcut. Since the tool and process parameters were the same as those used for machining the square pocket, it is reasonable to assume that the over-cut would remain unchanged. The square pocket was machined in 24 axial passes and its width was measured as 5.86 mm instead of the nominal value of 5 mm, *i.e.* the total overcut was 0.43 mm. This means that the overcut per axial pass was 0.018 mm. Hence, since the human-figured pocket was machined in twenty axial passes, the over-cut was assumed to be 0.36 mm. Therefore the outer boundary of the pocket was shrunk and the inner boundary defining the human figure expanded by this amount. The modified internal and external boundaries of the pocket were obtained using a CAD system (see dashed boundaries in Fig. 11(b)) and it was these expanded/shrunk boundaries that were used to generate the tool paths.

When machining an axial pass, the tool was constrained from moving in the vertical direction, as this would affect the inter-electrode gap. The consequence of this constraint is that the tool, after machining a region, could not be lifted, moved rapidly and then lowered to machine another region. Instead it had to be moved from one region to another, re-machining the material in between the two regions.

When generating contour-parallel tool paths, MASTERCAM could not generate the tool paths for the entire pocket in one stage as the human-shaped protrusion with its armpits and neck gave rise to concave regions. Offsets for the non-concave regions were generated in the first stage by successively offsetting the newly calculated outer boundary by 0.1 mm. These offsets are shown in Fig. 13(a). The last offset and the newly created inner boundary then gave rise to four concave regions labelled as I–IV in Fig. 13(a). In the second stage, offsets were generated for these four concave regions and they are shown for one of the four concave regions in Fig. 13(b).

MASTERCAM linked these offsets to generate a contour-parallel tool path for machining the pocket. Because of the four concave regions, the stock in every axial pass was removed in five steps. In the first step, all the offsets shown in Fig. 13(a) were machined, including the innermost offset which defined the shape of the protrusion (thick black profile in Fig. 14(a)). The position of the cutter at the end of the first step is also shown in Fig. 14(a).

The four regions were machined in the remaining steps. For example, in the second step, region I was machined and this required the cutter to traverse from A to B resulting in this portion of the inner boundary being re-machined (Fig. 14(b)). A similar situation arose when the cutter had to travel from the first region to the second (Fig. 14(c)) causing CD to be re-machined. Therefore linking the four regions without lifting the tool resulted in the complete inner boundary having to be re-machined.

The zigzag tool paths generated by MASTERCAM are shown in Fig. 15(a). These tool paths also gave rise to four concave regions but they were smaller in size. However the tool paths consisted solely of straight lines. One major difference between the contour-parallel and zigzag type of tool paths is that with the latter, the inner boundary was not completely machined in the first step (see the discontinuous thick black curve in Fig. 15(a)). As in the case of contour-parallel machining, linking the four regions caused the orange part of the inner profile to be re-machined.

To assess the machining accuracy, some dimensions of the machined pocket were measured and compared with nominal values. These were the width of the pocket at sections *A–A* (L4) and *B–B* (L5), the width of the leg (L2), the gap between the legs (L3) and the throat (L1) (see Fig. 11(b)). The actual and required values of these dimensions are shown in Table 3.

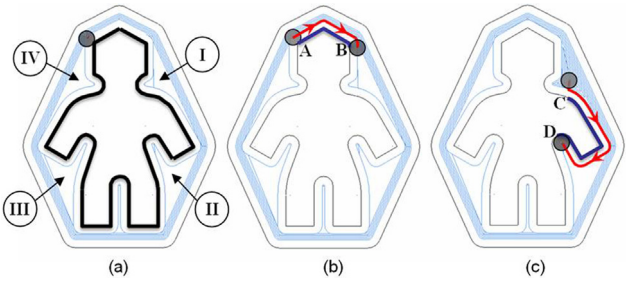

Fig. 14. Contour-parallel tool paths to link unmachined regions.

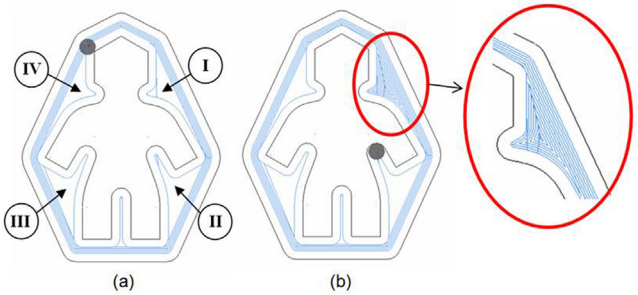

Fig. 13. (a) Unmachined regions and (b) the tool paths at region I.

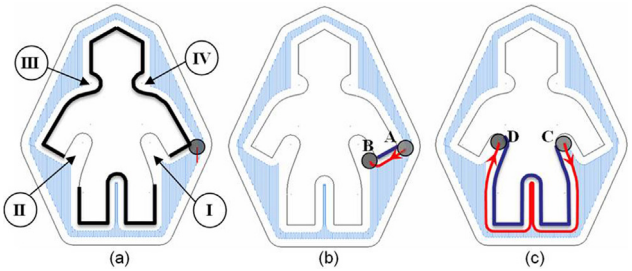

Fig. 15. Zig–zag tool paths to link unmachined regions.

Table 3
L1, L2, L3, L4 and L5 values of profile machined by zigzag and contour-parallel tool paths.

		Toolpath type			
	Nominal dimension	Zigzag	Error (%)	Contour-parallel	Error (%)
L1	1.8	1.76	2.22	1.78	1.11
L2	1.5	1.46	2.67	1.48	1.33
L3	2	2.03	1.50	2.04	2.00
L4	10.5	10.56	0.57	10.61	0.95
L5	12	12.16	1.33	12.08	0.67

On examining the results in Table 3, the following observations can be made.

(i) In some cases, when the errors arising from the two different types of tool paths are compared, one method does not appear to be clearly better than the other. For example, in the case of L4, zigzag tool paths result in an error of 0.57% whereas the error with contour parallel tool path is 0.95%. However, in the case of L5, the situation is reversed.
(ii) The errors relating to the inner boundary are greater than those relating to the outer boundary. For example, considering zig–zag tool paths, the errors associated with L1, L2 and L3 are 2.22, 2.67 and 1.5%, respectively, which are higher than those associated with L4 and L5. The reason for this is that these portions of the inner boundary were machined twice in every axial pass whereas in the case of L4 and L5, the outer boundary was machined only once.
(iii) In the case of L1 and L2, the error is negative whereas in the case of L3, L4 and L5 the error is positive. This means that the inner and outer boundaries have been over machined probably because the overcut has been under estimated.
(iv) The magnitude of the error varies from −0.02 and +0.16 mm.

The surface flatness of the pocket was another parameter that was examined. The cross-section profiles at *B–B* obtained with zigzag and contour-parallel tool paths are shown in Fig. 16. Both the curves are similar, with the base surface being concave and the walls slightly tapered. The concave nature of the base is not surprising because, as shown earlier, a cylindrical tool does not generate a flat surface. In the case of this pocket, consider the machining of the region around section *B–B* with zigzag tool paths. The tool travelled past points 1 and 5 on this section only once, point 2 six times, point 3 eleven times and point 4 eight times (see Fig. 17). Therefore, this unequal machining is the reason for the surface at *B–B* being concave.

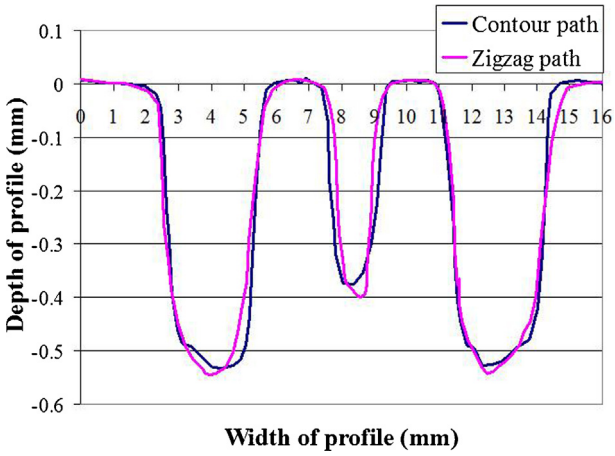

Fig. 16. Profile of the pockets at section *B–B*.

The step-over distance has a profound effect on the surface finish and the dimensions of the pocket. Using contour-parallel tool paths, when the step-over distance was changed from 0.1 mm to 0.3 mm, the base surface of the pocket was not as smooth, and this can be seen in Fig. 18(b). Measuring the surface roughness (R_a) with a laser profile-scanning machine, the average R_a values on the base surface of pocket surface using 0.1 and 0.3 mm step-over distances were 0.089 and 0.36, respectively.

When using zigzag tool paths, changing the step-over distance affects not only the base surface but also the profiles of the pocket. Fig. 19(b) shows the scallops that are present on the inner and outer boundaries of the pocket when using a step-over distance of 0.3 mm.

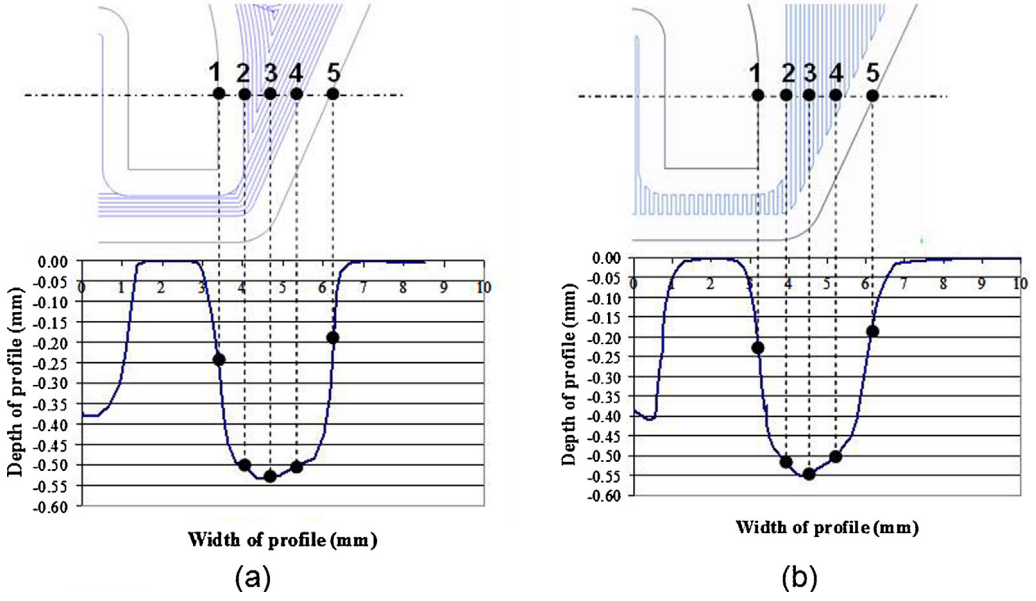

Fig. 17. Cross-section of the profile machined using (a) contour-parallel and (b) zig–zag tool paths.

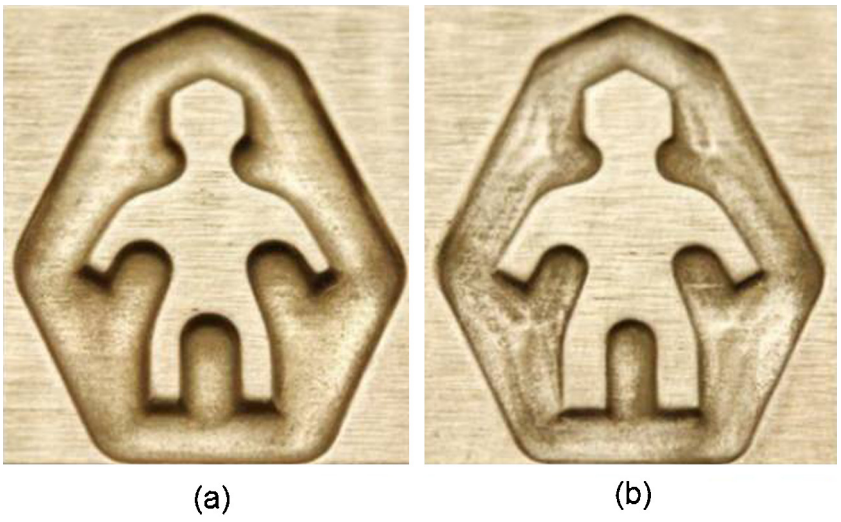

Fig. 18. Pockets machined using contour-parallel tool paths and different step-over distances (a) 0.1 mm and (b) 0.3 mm.

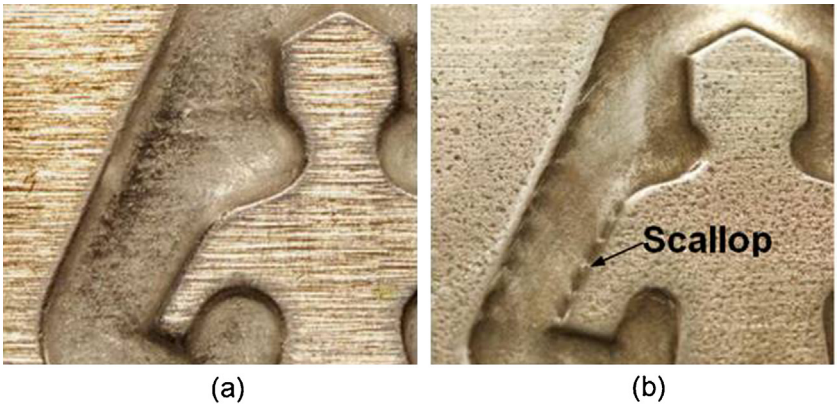

Fig. 19. Pockets machined using zig–zag tool paths and different step-over distances (a) 0.1 mm and (b) 0.3 mm.

Boundary elements results and discussion

Modelling the machining of a square pocket

To model the machining of the pocket by the BE method, the tool path shown in Fig. 7 was divided into small segments. The length of each segment depends on the time step which must be carefully chosen; it should not be too big otherwise oscillations in the workpiece profile will set in which may be difficult to dampen in subsequent iterations. From the results presented in [7], it was found that a time step of 0.1 s would be suitable for the BE model. Since the feed rate in the experimental tests was 9 mm/min, the tool path was divided into segments, each segment being 0.015 mm long as shown in Fig. 20.

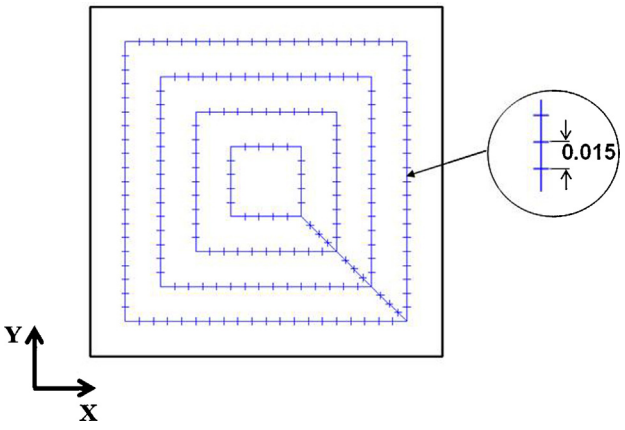

Fig. 20. Pocket tool path for BEM.

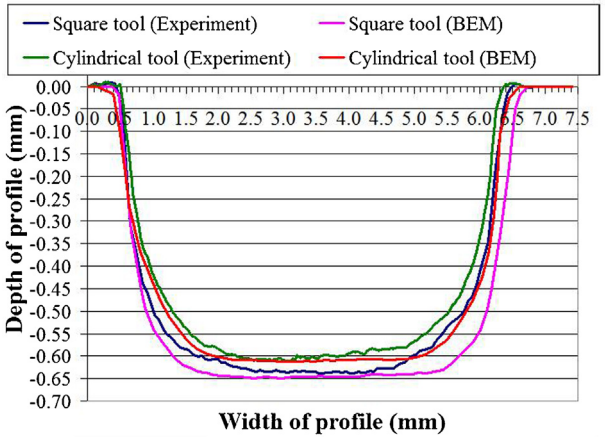

Fig. 21. Profiles of pockets machined by different tools.

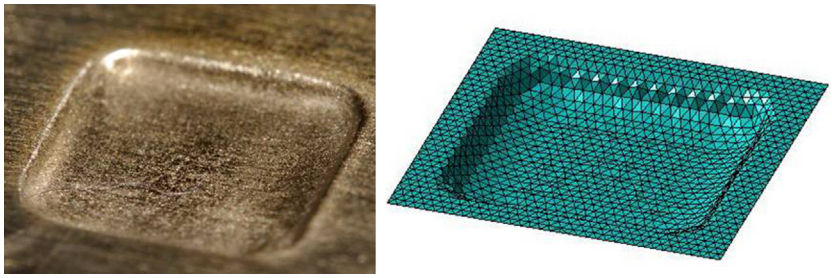

Fig. 22. Pocket machined by a cylindrical tool and predicted by the BEM.

Table 4
Comparison of value L1 to L5 obtained experimentally and from BE model.

	Contour-parallel					Zig–zag				
	L1	L2	L3	L4	L5	L1	L2	L3	L4	L5
BE model	1.65	1.31	2.18	11.2	12.81	1.62	1.28	2.21	11.2	13.1
Experiment	1.78	1.48	2.04	10.61	12.08	1.76	1.46	2.03	10.56	12.16
Error (%)	7.30	11.50	6.90	5.70	6.10	8.0	12.30	8.90	6.10	7.70

The cross-section profiles of the pockets obtained from the BEM are shown in Fig. 21; the experimental results are also included for the purpose of comparison. Fig. 22 shows the actual shape predicted by the BE model which is compared with that obtained experimentally.

The width and depth of the pocket obtained from the BE model were 6.22 and 0.65 mm, respectively, when machining with the square tool (Fig. 21) and 6.04 mm and 0.61 mm with the cylindrical tool. The cross-sectional profiles of the pockets predicted by the BE model for both the tools show good agreement with the experimentally measured profile, with the error being less than 3%.

Modelling of pocket with human-shaped protrusion machining

The EC machining of the human-shaped pocket was simulated using both zigzag and contour-parallel tool paths. To assess the accuracy of the model, values for L1 to L5 as obtained from the BE model are compared with the actual experimental values as shown in Table 4.

The average error with contour-parallel tool paths is smaller than that with zig–zig tool paths, the average error being 7.5 and 8.6%, respectively. However, when the actual profiles at section *B–B* are compared, the accuracy obtained at some parts of the profile is not good. The profiles predicted by the BE model for these two types of tool paths are shown in Figs. 23 and 24, whereas Fig. 25 shows the predicted and experimentally obtained shapes in 3D.

Figs. 24 and 25 also show the experimentally obtained profile. In both cases, the predicted profiles are slightly wider and deeper than the experimentally determined shape. Whilst the difference between the two predicted and experimental profiles may be acceptable at *A* and *C*, there is considerable error at *B*. Profile *B′–B–B″* corresponds to the gap between the legs which nominally should be 2 mm. The diameter of the cylindrical tool was 1 mm, which means that the gap between the sidewalls of the protrusion and the tool was only 0.5 mm. This small gap must have throttled the flow of the electrolyte causing some regions of the inter-electrode gap to be starved of the electrolyte. On the other hand, the model assumes ideal machining conditions *i.e.* the gap is filled with electrolyte. Since this most likely did not happen in reality, the model has over-estimated the amount of material dissolution. It is not realistic to model it as a coupled flow-cum-potential problem because modelling the flow in three dimensions would be very time consuming. It is unlikely that the presence of hydrogen bubbles and debris in the gap could have affected the overall electrical conductivity of the inter-electrode gap since a large quantity of the electrolyte was discharged from the nozzle.

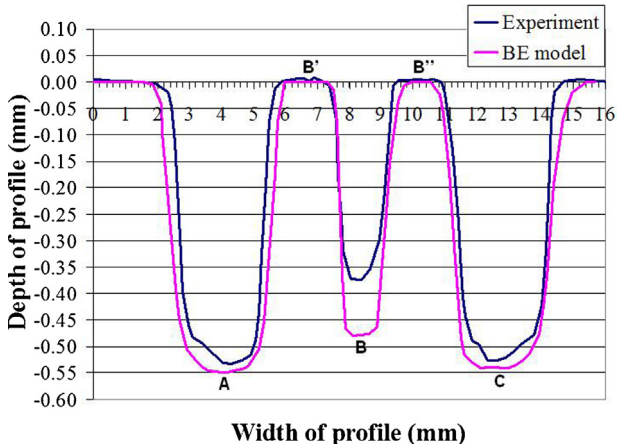

Fig. 23. Comparison of profiles obtained experimentally and from the BE model at section *B–B* using contour-parallel tool paths.

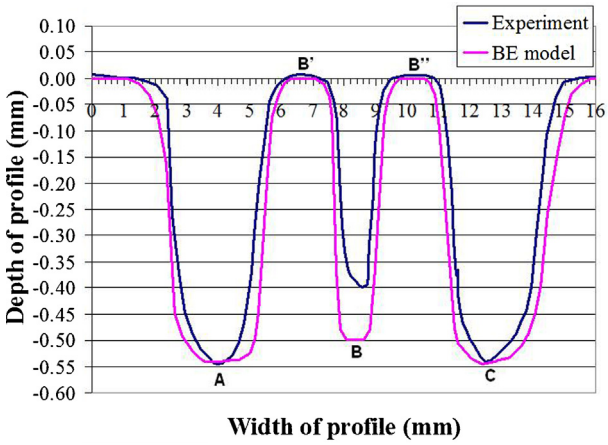

Fig. 24. Comparison of profiles obtained experimentally and from the BE model at section BB using zig–zag tool paths.

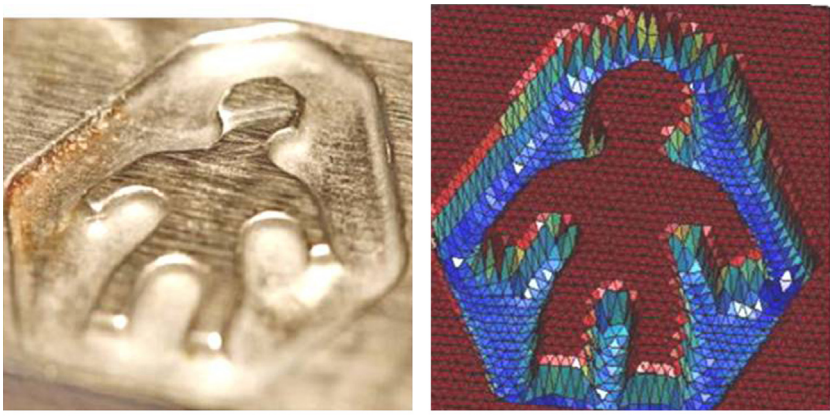

Fig. 25. 3D view of the pocket obtained (a) experimentally and (b) from BE model.

Conclusion

The investigations reported herein have shown that EC milling of certain features like slots and pockets is feasible with tools of very simple geometry. However, the accuracy obtained will depend on the shape of the tool and *a priori* knowledge of the overcut. The tool shape affects the flatness of the base surface. There was always a blend between a sidewall and the base face.

Comparing the type of tool paths, both the zigzag and contour-parallel tool paths resulted in features of similar surface finish and accuracy. However, the zigzag tool paths were shorter than the contour-parallel tool paths in the case of the pocket with the human-shaped figure. If the radial width of cut is large, then, with zigzag tool paths, the side faces become scalloped whereas the base face becomes scalloped with contour-parallel tool paths.

Generally speaking, the profile shapes predicted by the BE model were in good agreement with the actual machined workpiece. However, if the machined feature becomes deep and narrow, the accuracy decreases resulting in the BE model predicting a deeper and wider feature probably because it assumes ideal machining conditions.

The analysis of the pocket with the human-figure protrusion has shown that there is a need for a CAM software specially tailored for EC machining. This software should be able to offset a boundary of the workpiece by a specified amount. The tool paths should be continuous even if there are concave regions. This could be achieved by more intelligent linking of the offsets. This CAM software should minimise the amount of re-machining. However, if a segment of a tool path has to be re-machined, then the re-machining must be carried out at a high feed rate so that very little material dissolution takes place.

If more than one workpiece is being machined, then, if necessary, the overcut should be revised for the second and subsequent workpieces, and the tool paths recalculated so that the second and subsequent machined workpiece dimensions are closer to those required.

References

[1] Kozak, J., Rajurkar, K.P., Makkar, Y., 2004, Study of pulse electrochemical micromachining, J Manuf Processes, 6:7–14.
[2] Kim, B.H., Ryu, S.H., Choi, D.K., Chu, C.N., 2005, Micro electrochemical milling, J Micromech Microeng, 15:124–129.
[3] Hackert-Oschätzchen, M., Meichsner, G., Zinecker, M., Martin, A., Schubert, A., 2012, Micro machining with continuous electrolytic free jet, Precis Eng, 36:612–619.
[4] Zeng, Z., Wang, Y., Wang, Z., Shan, D., He, X., 2012, A study of micro-EDM and micro-ECM combined milling for 3D metallic micro-structures, Precis Eng, 36:500–509.
[5] Kozak, J., Chuchro, M., Ruszaj, A., Karbowski, K., 2000, The computer aided simulation of electrochemical process with universal spherical electrodes when machining sculptured surfaces, J Mater Process Technol, 107:283–287.
[6] Ruszaj, A., Zybura-Skrabalak, M., 2001, The mathematical modelling of electrochemical machining with flat ended universal electrodes, J Mater Process Technol, 109:333–338.
[7] Pattavanitch, J., Hinduja, S., Atkinson, J., 2010, Modelling of the electrochemical machining process by the boundary element method, CIRP Ann—Manuf Technol, 59/1:243–246.
[8] Vanderauwera, W., Vanloffelt, M., Perez, R., Lauwers, B., 2013, Investigation on the performance of macro electrochemical milling, The Seventeenth CIRP Conference on Electro Physical and Chemical Machining (ISEM), 6:357–362.
[9] Hewson-Browne, R.C., 1971, Further applications of complex variable methods to electrochemical machining problems, J Eng Math, 5:233–240.
[10] Loutrel, S.P., Cook, N.H., 1973, A theoretical model for high rate electrochemical machining, J Eng Ind Trans ASME, 95/4: 1003–1008.
[11] Tipton, H., 1964, The dynamics of electrochemical machining, Proc. 5th Int. MTDR Conf, University of Birmingham, Birmingham.
[12] Kozak, J., 1998, Mathematical models for computer simulation of electrochemical machining processes, J Mater Process Technol, 76:170–175.
[13] Jain, V.K., Pandey, P.C., 1980, Finite element approach to the two-dimensional analysis of electrochemical machining, Prec Eng, 2:23–28.
[14] Alkire, R., Bergh, T., Sani, R.L., 1978, Predicting electrode shape change with use of finite element methods, J Electrochem Soc, 125:1981–1988.
[15] Narayanan, O.H., Hinduja, S., Noble, C.F., 1986, The prediction of workpiece shape during electrochemical machining by the boundary element method, Int J Mach Tool Des Res, 26:323–338.
[16] Deconinck, J., 1992, Current Distributions and Electrode Shape Changes in Electrochemical Systems, Springer-Verlag, Berlin, Heidelberg/New York.
[17] McGeough, J.A., 1974, Principles of Electrochemical Machining, Chapman and Hall, London.
[18] Held, M., 1991, On the Computational Geometry of Pocket Machining, Springer, Berlin.
[19] Hinduja, S., Mansor, M.S.A., Owodunni, O.O., 2010, Voronoi-diagram-based linking of contour-parallel tool paths for two and a half-dimensional closed pocket machining, Proc Inst Mech Eng B: J Eng Manuf, 224/9:1329–1350.